Modulation of whistler mode chorus waves: 1. Role of compressional Pc4–5 pulsations

W. Li,[1] R. M. Thorne,[1] J. Bortnik,[1] Y. Nishimura,[1,2] and V. Angelopoulos[3]

Received 1 December 2010; revised 1 February 2011; accepted 21 March 2011; published 9 June 2011.

[1] Using observations from the THEMIS spacecraft, we investigate the modulation of whistler mode chorus waves in the magnetosphere by compressional Pc4–5 pulsations (i.e., pulsations with periods from tens of seconds to a few minutes) with an anticorrelation between the total electron density and the background magnetic field intensity. We find that such compressional pulsations are associated with modulations of resonant electron fluxes and chorus intensity. Changes in the total electron density, background magnetic field, and the flux and anisotropy of resonant electrons could all be responsible for triggering the excitation of chorus waves. To quantitatively investigate which parameters dominantly contribute to chorus generation, we evaluate the changes in linear growth rates of whistler mode waves due to variations in either the ratio of resonant electrons to the total electrons $R(V_R)$ or the electron anisotropy $A(V_R)$. In the majority of cases, the modulation of whistler mode wave intensity is dominated by $R(V_R)$ variations caused by compressional Pc4–5 pulsations and tends to occur at large L shells of 8–12 in the dawn sector. Only a small fraction of events are associated with $A(V_R)$ modulations and these typically occur at lower L shells (<~8).

Citation: Li, W., R. M. Thorne, J. Bortnik, Y. Nishimura, and V. Angelopoulos (2011), Modulation of whistler mode chorus waves: 1. Role of compressional Pc4–5 pulsations, *J. Geophys. Res.*, *116*, A06205, doi:10.1029/2010JA016312.

1. Introduction

[2] Whistler mode chorus waves in the extremely low frequency (ELF) and very low frequency (VLF) range, i.e., between a few hundreds Hz and several kHz, are excited in the low-density region outside the plasmapause from the premidnight to the afternoon sector by the injection of the anisotropic plasma sheet electrons [e.g., *Burtis and Helliwell*, 1969; *Tsurutani and Smith*, 1974; *Meredith et al.*, 2003]. The frequency of chorus emissions scales with the equatorial electron cyclotron frequency (f_{ce}), typically occurring at frequencies of 0.1–0.8 f_{ce} [e.g., *Helliwell*, 1967; *Burtis and Helliwell*, 1969; *Tsurutani and Smith*, 1977; *Santolík et al.*, 2004]. Chorus emissions are commonly observed in two distinct frequency bands (lower band and upper band) with a minimum wave power near 0.5 f_{ce} [*Tsurutani and Smith*, 1974; *Koons and Roeder*, 1990]. The source region of whistler mode chorus waves is generally believed to be located near the geomagnetic equator [e.g., *LeDocq et al.*, 1998; *Lauben et al.*, 2002; *Santolík et al.*, 2003], although several studies reported observations of chorus waves with a probable source at high latitudes on the dayside [e.g., *Vaivads et al.*, 2007; *Tsurutani et al.*, 2009]. It is generally accepted that whistler mode chorus waves are generated through a cyclotron resonance with anisotropic electrons with energies between a few and tens of keV [e.g., *Kennel and Petschek*, 1966; *Kennel and Thorne*, 1967; *Tsurutani and Smith*, 1974; *Nunn et al.*, 1997; *Omura et al.*, 2008; *Li et al.*, 2008, 2009a], although the precise details of the excitation process remain a topic of intense research [e.g., *Omura et al.*, 2009; *Bespalov et al.*, 2010; *Schriver et al.*, 2010; *Santolík et al.*, 2010; *Lampe et al.*, 2010, and references therein].

[3] Chorus consists of discrete elements, each of which lasts for a time on the order of a tenth to a few tenths of a second [e.g., *Santolík et al.*, 2003]. These individual chorus elements are frequently clustered together and modulated on timescales from a few seconds to a few minutes. Previous observations on the ground have shown that the intensities of VLF radio emissions are often modulated at ultra low frequencies (ULF) [*Helliwell*, 1965; *Kimura*, 1974; *Sato et al.*, 1974; *Sato and Fukunishi*, 1981]. It has been proposed that quasi-periodic whistler emissions originate in the magnetosphere and are the result of the modulation of an existing VLF hiss or chorus source in the equatorial plane of the magnetosphere by the compressional components of ULF waves [*Coroniti and Kennel*, 1970; *Sato and Fukunishi*, 1981]. *Tixier and Cornilleau-Wehrlin* [1986] observed events near the equatorial plane using the GEOS satellite and showed that VLF modulation seemed to be controlled by a compressional component of ULF waves. More recently, *Manninen et al.* [2010] suggested that modulations of particle precipitation

[1]Department of Atmospheric and Oceanic Sciences, University of California, Los Angeles, California, USA.
[2]Solar-Terrestrial Environment Laboratory, Nagoya University, Nagoya, Japan.
[3]Institute of Geophysics and Planetary Physics, Department of Earth and Space Sciences, University of California, Los Angeles, California, USA.

0148-0227/11/2010JA016312

and whistler mode chorus are caused by the 2.0 mHz compressional component of Pc5 poloidal geomagnetic pulsations.

[4] Compressional Pc4–5 pulsations with periods ranging from a few tens of seconds to more than 600 s are common on the nightside toward the two flanks of the magnetosphere in both the dusk and dawn sectors in the spatial region beyond $L = 8$ at low geomagnetic latitudes [e.g., *Hedgecock*, 1976; *Baumjohann et al.*, 1987; *Takahashi et al.*, 1990; *Anderson et al.*, 1990; *Zhu and Kivelson*, 1991; *Vaivads et al.*, 2000, 2001]. The generation of compressional pulsations in the Pc4–5 range has been associated with various magnetospheric processes, which may be divided into external processes related to the solar wind flow [e.g., *Kepko and Spence*, 2003; *Han et al.*, 2007; *Kessel*, 2008], and internal magnetospheric processes such as drift mirror mode instability [e.g., *Hasegawa*, 1969; *Cheng and Lin*, 1987; *Korotova et al.*, 2009]. The mirror mode is generated by plasma pressure anisotropies, when the plasma β (ratio of plasma pressure to magnetic pressure) is large (>1) [e.g., *Hasegawa*, 1969; *Patel et al.*, 1983; *Price et al.*, 1986; *Southwood and Kivelson*, 1993; *Kivelson and Southwood*, 1996; *Zhu and Kivelson*, 1994; *Rae et al.*, 2007]. Mirror mode waves are typically associated with an antiphase relation in magnetic and plasma pressure, which maintains quasi-equilibrium of the total pressure [e.g., *Zhu and Kivelson*, 1991; *Vaivads et al.*, 2001; *Rae et al.*, 2007; *Korotova et al.*, 2009].

[5] Electron fluxes responsible for chorus generation can be modulated by ULF waves in the Pc4–5 range as demonstrated in a number of ground-based, satellite, and theoretical studies [e.g., *Kokubun et al.*, 1977; *Kremser et al.*, 1981; *Spanswick et al.*, 2005; *Sarris et al.*, 2007]. Pc5 pulsations can modulate the flux of suprathermal particles (>50 keV) in the region of 6–11 R_E preferentially near the dawn and noon-dusk sectors and the relative phase of variation is found to depend on the energy of the particles [e.g., *Kokubun et al.*, 1977]. In the events analyzed by *Baumjohann et al.* [1987], both energetic proton and electron fluxes (a few eV to tens of keV) are anticorrelated with the compressional magnetic field oscillations. More recently, *Sarris et al.* [2007] showed electron flux modulations at the magnetospheric pulsation frequency as well as at various other frequencies in the Pc4–5 range related to the drift frequencies of the particles and their harmonics. Modulation of such energetic electrons by ULF waves can be expected to modulate the chorus intensity by changing resonant electron fluxes, which affect the growth rate of chorus waves.

[6] Although the idea of VLF power modulation by ULF waves has been proposed for several decades, most previous studies were performed using ground-based measurements at high latitude stations. Direct studies on the modulation of VLF waves by compressional Pc4–5 pulsations in the equatorial magnetosphere are very limited. Previous studies [e.g., *Meredith et al.*, 2003; *Li et al.*, 2009b] have shown that the wave power of nightside chorus is mainly confined within 15° of the magnetic equator and becomes weaker at higher magnetic latitudes. Thus only a portion of whistler mode chorus is able to propagate to high latitudes and be measured on the ground. Chorus waves observed near the source region in the magnetosphere and on the ground could be quite different. Because Landau damping often extinguishes the chorus waves before they reach midlatitudes [e.g., *Bortnik et al.*, 2007; *Li et al.*, 2008] and the ionosphere damps the waves significantly even if chorus can impinge on the ionosphere [e.g., *Starks et al.*, 2008]. On the other hand, some compressional waves in the magnetosphere are shielded by the ionosphere and cannot be observed on the ground [*Hughes and Southwood*, 1976]. Since chorus waves are preferentially generated near the equator [e.g., *LeDocq et al.*, 1998; *Lauben et al.*, 2002; *Santolík et al.*, 2003] and compressional Pc4–5 pulsations also tend to be localized at low magnetic latitudes [e.g., *Takahashi et al.*, 1990; *Zhu and Kivelson*, 1991], it is essential to investigate whistler mode chorus modulation by compressional waves in the equatorial magnetosphere.

[7] The main objective of this study is to evaluate the role of compressional Pc4–5 pulsations exhibiting an antiphase relation between the total electron density and the magnetic field in whistler mode wave modulation. We utilize simultaneous observations of wave and particle distributions in the near-equatorial magnetosphere by the THEMIS satellites. In this paper we address chorus power modulation in the Pc4–5 range, while the study of shorter timescale modulations is left for a companion paper of *Li et al.* [2011]. In situ observations of the total density, ambient magnetic field intensity and resonant electron flux are used to determine how the modulation of those parameters by compressional Pc4–5 pulsations correlate with chorus wave intensities. We further calculate wave growth rates using linear theory to investigate which parameters dominantly contribute to the wave generation. In Sections 2 and 3, we briefly describe our analysis of the THEMIS data and the calculation of linear growth rates respectively. In Section 4, two events of chorus modulation by compressional pulsations are analyzed in detail and compared to variations in the linear wave growth rates, which is followed by statistical results on the global distribution of these events. In Sections 5 and 6 we discuss and summarize the principal results of the present study.

2. THEMIS Data Analysis

[8] The THEMIS spacecraft, comprising 5 probes in near-equatorial orbits with apogees above 10 R_E and perigees below 2 R_E [*Sibeck and Angelopoulos*, 2008] are well situated and instrumented to measure key parameters related to the modulation of whistler mode waves including background magnetic fields, total electron densities, and electron distributions in the dominant chorus source region.

[9] The Electrostatic Analyzer (ESA) is designed to measure the ion and electron distributions over the energy range from a few eV up to 30 keV for electrons, and up to 25 keV for ions [*McFadden et al.*, 2008]. The instrument consists of a pair of "top hat" electrostatic analyzers with common 180° × 6° fields of view that sweep out 4π steradians in each 3 s spin period. The Solid State Telescope (SST) measures superthermal particles from 25 keV up to 6 MeV for ions and up to ~900 keV for electrons [*Angelopoulos*, 2008]. Therefore, ESA and SST data in our study are utilized to provide information on the energy flux and pitch angle distribution of electrons covering a broad energy range. Radiation belt contamination is removed from the original ESA data by subtracting minimum count rates, which are essentially independent of energy. Furthermore, the total plasma pres-

sure is calculated by the sum of the ion and electron thermal pressures measured from both ESA and SST in this study.

[10] The Fluxgate Magnetometer (FGM) [*Auster et al.*, 2008] measures background magnetic fields and their low frequency fluctuations (up to 64 Hz) in the near-Earth space. The Electric Field Instrument (EFI) measures three components of the ambient vector electric fields [*Bonnell et al.*, 2008]. Individual sensor potentials are also measured, providing on-board and ground-based estimation of spacecraft floating potential and high-resolution plasma density measurements [*Bonnell et al.*, 2008]. The total electron density can be inferred from the spacecraft potential and the electron thermal speed measured by the EFI and ESA instruments respectively, including the cold plasma population in addition to the hot plasma component measured by ESA. The electron density outside of the plasmapause is calibrated by a statistical comparison with 2 years of ESA observations for each spacecraft. Details of the method are described by *Mozer* [1973] and *Pedersen et al.* [1998], and the electron densities obtained are associated with an uncertainty generally within a factor of ~2. Note that all electron density data used in this study is inferred from the spacecraft potential.

[11] The Search Coil Magnetometer (SCM) [*Roux et al.*, 2008; *Le Contel et al.*, 2008] measures low-frequency magnetic field fluctuations and waves in three orthogonal directions over a frequency range from 0.1 Hz to 4 kHz. EFI provides waveforms and three-axis spectral measurements of ambient electric fields from DC up to 8 kHz. The SCM and EFI output waveforms are digitized and processed by the Digital Fields Board (DFB) [*Cully et al.*, 2008]. The root mean square amplitudes at various wide frequency bands (from the filter bank data product) are included in the survey mode telemetry, covering most orbits with a measurement cadence of four seconds in six logarithmically spaced frequency bands in a range of 2 Hz–4 kHz. In addition to survey products, the DFB outputs high-resolution spectra in the particle burst mode with up to 64-bin resolution in wave frequency with a cadence of 1 s. Furthermore, waveforms of the 3 magnetic and electric field components at up to 16 kHz sampling frequency are captured in the wave burst mode.

[12] Equipped with the high-quality electric field (EFI), magnetic field (SCM), and particle (ESA and SST) instruments, the THEMIS spacecraft offer an excellent opportunity to study characteristics of the whistler mode chorus wave and key parameters related to its modulation in the dominant wave generation region.

3. Linear Growth Rates

[13] In this study, linear growth rates of whistler mode waves have been calculated based on the measured parameters on THEMIS and compared to the observed wave amplitude. The local growth rates (γ) of weakly growing, parallel propagating whistler mode chorus can be calculated by equation (1) using linear theory [*Kennel and Petschek*, 1966]:

$$\gamma = \pi|\Omega_e|\left(1-\frac{\omega}{|\Omega_e|}\right)^2 \eta(V_R)\cdot[A(V_R)-A_c], \tag{1}$$

where Ω_e is the electron cyclotron frequency and ω is the wave frequency, $V_R = \frac{\omega-|\Omega_e|}{k}$ is the nonrelativistic, parallel velocity of electrons resonating with whistler waves through the first-order resonance, and k is the wave number. Here

$$\eta(V_R) = 2\pi\frac{|\Omega_e|-\omega}{k}\cdot\int_0^\infty v_\perp dv_\perp f\left(v_\perp, v_\parallel = V_R\right) \tag{2}$$

is the ratio of resonant electrons to total electrons. In equation (2) f is the electron phase space density (PSD), and $v_\parallel$ and $v_\perp$ are electron velocity parallel and perpendicular to the ambient magnetic field. The critical anisotropy (A_c) for instability is equal to $\frac{1}{|\Omega_e|/\omega-1}$, and the electron anisotropy for a fixed resonant velocity can be expressed as

$$A(V_R) = \left.\frac{\int_0^\infty v_\perp dv_\perp\left(v_\parallel\frac{\partial f}{\partial v_\perp} - v_\perp\frac{\partial f}{\partial v_\parallel}\right)\frac{v_\perp}{v_\parallel}}{2\int_0^\infty f v_\perp dv_\perp}\right|_{v_\parallel = V_R}. \tag{3}$$

Following *Kennel and Petschek* [1966], we define

$$R(V_R) = \left(1-\frac{\omega}{|\Omega_e|}\right)^2\eta(V_R), \tag{4}$$

then equation (1) can be expressed as

$$\frac{\gamma}{|\Omega_e|} = \pi\cdot R(V_R)\cdot[A(V_R)-A_c]. \tag{5}$$

In order to obtain positive wave growth, $A(V_R)$ must be larger than A_c. The rate of growth or damping depends on both $A(V_R)$ and $R(V_R)$. A_c is larger at higher normalized wave frequency, which means that generation of waves with a higher normalized frequency requires a larger anisotropy.

[14] Using the simple estimate of whistler wave growth rates presented above, we examine the THEMIS data to determine the parameters that are expected to dominantly control chorus modulation.

4. Results of the Data Analysis

[15] Two typical cases are presented first, to demonstrate the role of compressional Pc4–5 pulsations in whistler mode wave modulation. In order to determine the preferential region and plasma conditions for chorus modulation by compressional pulsations, a statistical analysis has also been performed. The solar wind data shifted to the bow shock nose used in this study was obtained from the OMNI website and the interplanetary magnetic field (IMF) is shown in GSM coordinates. The AE index with a 1 min time resolution was provided by the World Data Center for Geomagnetism, Kyoto.

4.1. Case 1

[16] Figures 1a and 1b show the solar wind dynamic pressure and IMF B_y (blue) and B_z (red) in Case 1, which were measured between 09:00 and 12:15 UT on 15 December 2008. During this period, the solar wind dynamic pressure was low (1–2 nPa) without a significant variation, the magnitude of B_z was small, less than ~2 nT, and B_y mostly remained negative. The AE index is shown in Figure 1c. The geomagnetic activity was quiet with the Kp

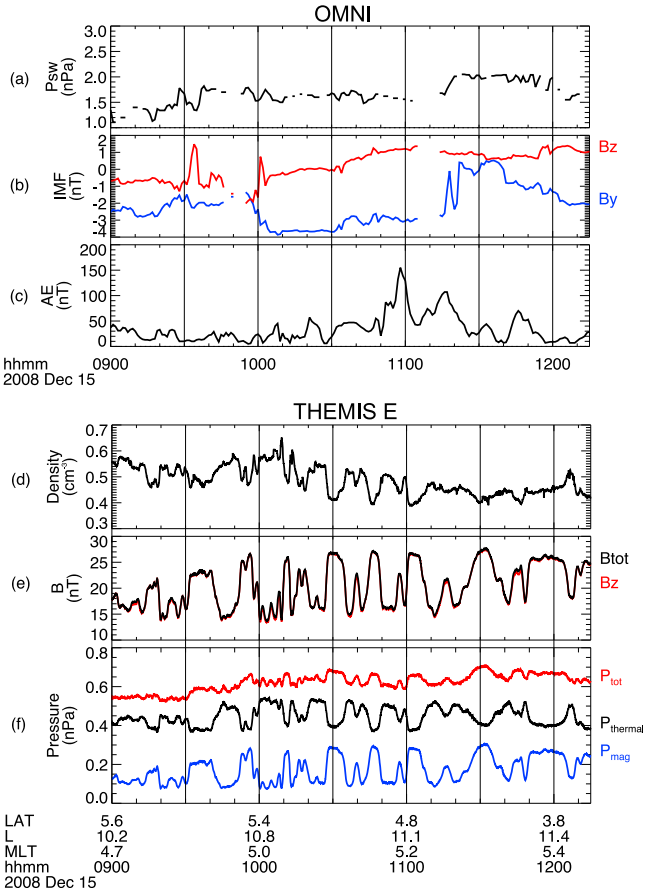

Figure 1. (a) Solar wind dynamic pressure, (b) IMF B_y (blue) and B_z (red) shifted to bow shock nose, and (c) AE index during 09:00–12:15 UT on 15 December 2008. (d) Total electron density inferred from the spacecraft potential, (e) total background magnetic field (black) and magnetic field in the z direction in the SM coordinate system (red), (f) thermal plasma pressure (black), magnetic pressure (blue), and total pressure (red) observed by THEMIS E during the same time interval.

index of 0+ (not shown) and AE values were generally low, less than ~160 nT.

[17] Figures 1d–1f show the total electron density inferred from the THEMIS spacecraft potential, the background magnetic fields (total magnetic field B_{tot} and B_z in the SM coordinate system), and the pressures observed by THEMIS E during the same time interval. The total pressure (red) is the sum of the magnetic pressure (blue) and the thermal pressure (black), which includes ion and electron pressures measured from both ESA and SST. Note that B_z was almost the same as B_{tot}, indicating that the total variation in magnetic field mainly occurred in the z direction. Therefore, these waves can be identified as compressional waves, and exhibit a period of a few minutes. The total electron density (Figure 1d) and background magnetic field (Figure 1e) were well correlated and out of phase. The plasma and magnetic pressures were also out of phase (Figure 1f), and thus tended to maintain the total pressure quasi-equilibrium. The thermal plasma pressure was significantly larger than the magnetic pressure with a mean value of $\beta \sim 3.1$ and occasionally reaching values as high as ~8.

[18] These compressional pulsations occurred near the dawn sector (4.7–5.4 MLT) at large L shells (10.2–11.4). During this time period, the compressional Pc4–5 pulsations were not associated with the variations in solar wind dynamic pressure or IMF, as seen from Figures 1a and 1b. These compressional waves in the outer magnetosphere were not likely to be related to intervals of enhanced geomagnetic activity, but they were present in inhomogeneous high β plasmas ($\beta > 1$), consistent with *Zhu and Kivelson* [1994] and *Korotova et al.* [2009]. All the features in Case 1 are similar to the compressional pulsation event shown by *Korotova et al.* [2009], which occurred in the dawnside magnetosphere (4.4–5.1 MLT) at L shells of 11–13.5. These compressional Pc4–5 waves in Case 1 may be locally driven by the drift mirror instability as suggested by *Hasegawa* [1969], *Cheng and Lin* [1987], and *Korotova et al.* [2009], and they do not appear to be directly related to upstream solar wind conditions.

[19] Figure 2 shows the key parameters that are potentially responsible for the whistler mode wave modulation observed by THEMIS E in Case 1. Figures 2a and 2b show the total electron density and ambient magnetic field, same as in Figures 1d and 1e, in order to compare with variations of other parameters for convenience. The evolution of the omnidirectional electron energy flux and electron anisotropy is shown in Figures 2c and 2d respectively. Electron anisotropy (A^*) is calculated for a fixed electron kinetic energy [e.g., *Chen et al.*, 1999] as follows:

$$A^* = \frac{\int_0^{\pi/2} f(E,\alpha_0)\sin^3\alpha_0 d\alpha_0}{2\int_0^{\pi/2} f(E,\alpha_0)\cos^2\alpha_0 \sin\alpha_0 d\alpha_0} - 1, \quad (6)$$

where α_0 is the equatorial pitch angle, E is the electron kinetic energy, and f is the electron PSD. $A^* = 0$ corresponds to pitch angle isotropy, $A^* > 0$ represents pitch angle distribution peaked at 90°, while $A^* < 0$ indicates a PSD minimum at 90°. Electron anisotropy (A^*) was generally positive at energies larger than ~1 keV, but tended to be smaller or even negative at lower energies (<~1 keV). Figure 2e shows electron energy fluxes over the energy of 3–30 keV roughly perpendicular (blue) and parallel (black) to the ambient magnetic field. These electron fluxes include the main population of electrons that are able to resonate with the observed whistler mode waves as we discussed below. Variations of both perpendicular and parallel electron energy fluxes were roughly out of phase with the background magnetic field and in phase with the total electron density. Figure 2f shows the minimum energy of nonrelativistic electrons which undergo the first-order cyclotron resonance with the parallel propagating whistler mode waves, expressed as [*Kennel and Petschek*, 1966]

$$E_{\min}^{\text{Cyclotron}} = \frac{B^2}{8\pi N}\frac{\Omega_e}{\omega}\left(1 - \frac{\omega}{\Omega_e}\right)^3. \quad (7)$$

Here N is the total electron density and B is the ambient magnetic field. The minimum resonant energy varied in phase with the background magnetic field and out of phase with the

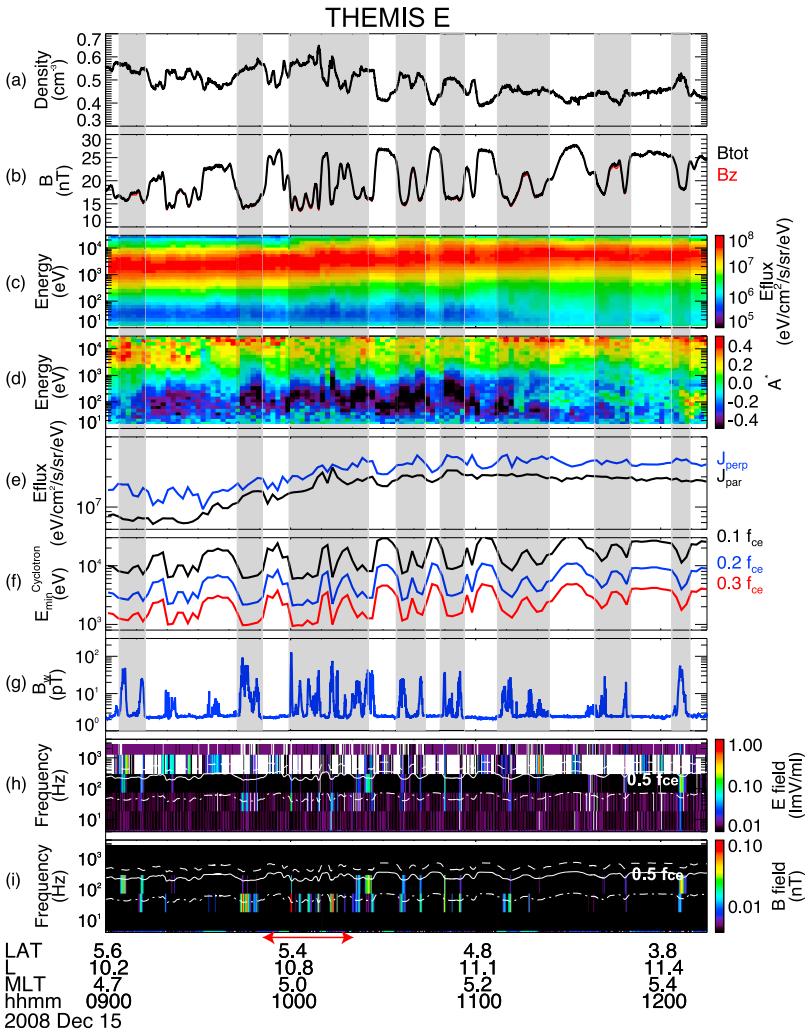

Figure 2. Case 1 observed by THEMIS E between 09:00 and 12:18 UT on 15 December 2008 during the fast survey. (a) Total electron density, (b) total magnetic field (black) and magnetic field in the *z* direction in the SM coordinate (red). (c) Omnidirectional electron energy flux and (d) electron anisotropy (A^*) as functions of energy and time. (e) Electron energy flux over the energy of 3–30 keV perpendicular (blue) and parallel (black) to the background magnetic field, (f) Minimum resonant energy of electrons interacting with waves of three normalized frequencies through the first-order cyclotron resonance, (g) root mean square of wave magnetic field amplitude over the frequency band of 0.05–0.8 f_{ce}, and time-frequency spectrograms of (h) wave electric and (i) magnetic fields. The three white lines in Figures 2h and 2i represent 1 f_{ce} (dashed), 0.5 f_{ce} (solid), and 0.1 f_{ce} (dashed-dotted).

total electron density, as can be inferred from equation (7). The anticorrelation between B and N is particularly efficient in modulating the minimum resonant energy, since the observed change of both macroscopic properties enhance the change in minimum resonant energy in the same direction. Figures 2h and 2i show time-frequency spectrograms of the wave amplitude in electric and magnetic fields respectively. The root mean square of the wave magnetic field amplitude over the frequency of 0.05–0.8 f_{ce} in Figure 2i was calculated and is shown in Figure 2g. Interestingly, the comparison of Figures 2f and 2g shows that the amplitude of whistler mode waves increases (decreases) when the minimum resonant energy decreases (increases). This is consistent with theoretical estimates, since the resonant electron phase space density for the lower minimum resonant energy is larger, thus contributing to the increase in wave growth rates and vice versa.

[20] During the time interval from 09:55 to 10:18 UT (marked by the horizontal red arrow below) particle burst data was available and provided particle and wave data with higher resolution in time and frequency. Figure 3 shows similar parameters as shown in Figure 2 but during the shorter interval. Figures 3a and 3b show the compressional Pc4–5 pulsations with an antiphase relationship between the total electron density and ambient magnetic field with a time period of a few minutes. Figure 3e shows that resonant electron fluxes (3–30 keV) were modulated by the compressional pulsations in phase with the total electron density and out of phase with the magnetic field. Figure 3f shows the minimum resonant energy for electrons interacting with whistler mode waves with three frequencies of 0.1 (black), 0.2 (blue), and 0.3 f_{ce} (red). The minimum resonant energies changed substantially, by a factor of up to ~3, due to the

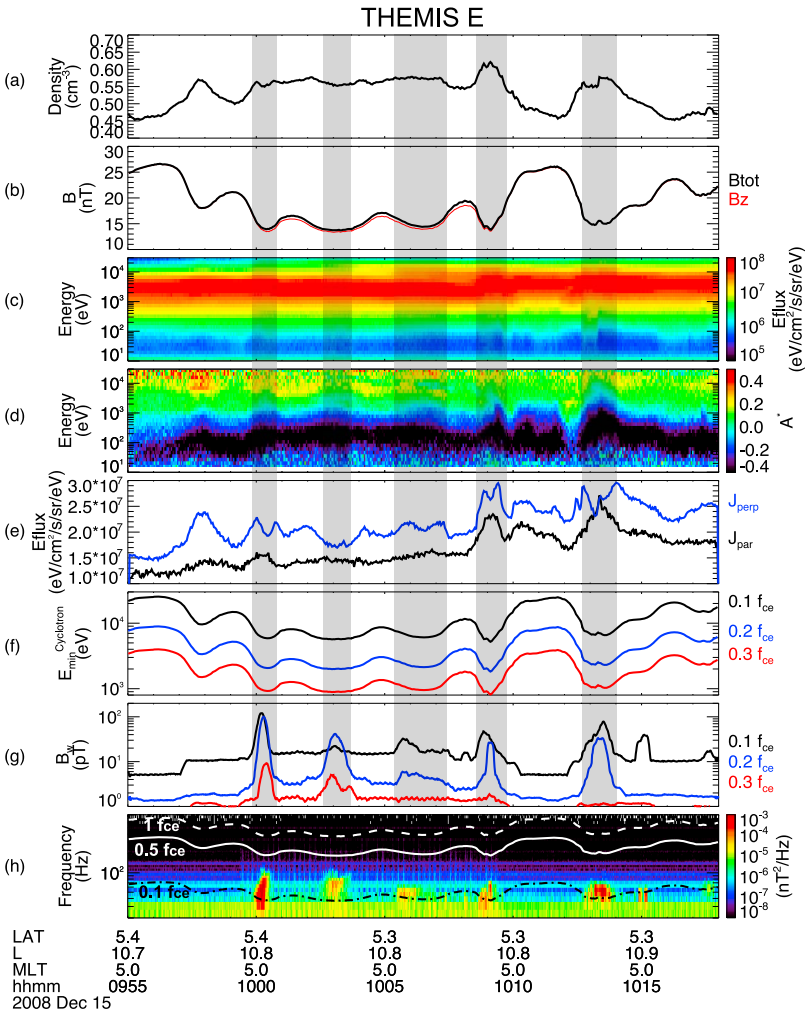

Figure 3. Case 1 observed by THEMIS E between 09:55 and 10:18 UT on 15 December 2008 during a period when particle burst data was available. (a–f) Same format as in Figures 2a–2f. (g) Integrated chorus wave amplitude over 0.05–0.15 f_{ce} (black), 0.15–0.25 f_{ce} (blue), and 0.25–0.35 f_{ce} (red), and (h) time-frequency spectrogram of the wave magnetic field spectral intensity. Two white lines in Figure 3h represent 1 f_{ce} (dashed), 0.5 f_{ce} (solid), and the black line (dashed-dotted) indicates 0.1 f_{ce}.

modulations of the electron density and magnetic field. In Figures 3e, resonant electron fluxes are integrated over the energy range from 3 to 30 keV, since the minimum resonant energy for the observed wave frequency (mostly less than 0.2 f_{ce}) is ~3 keV in Figure 3f. Figure 3e shows that the perpendicular resonant electron flux was larger than the parallel electron flux, which provides favorable conditions for whistler mode wave generation [e.g., *Kennel and Petschek*, 1966]. Figure 3h shows the modulated wave magnetic field spectral intensity. The wave magnetic field spectral intensity was integrated over 0.05–0.15 f_{ce} (black), 0.15–0.25 f_{ce} (blue), and 0.25–0.35 f_{ce} (red) and the corresponding wave amplitudes at different frequencies are shown in Figure 3g. The comparison clearly shows that the amplitude of whistler mode waves (Figure 3g) positively correlates with variations in the total electron density (Figure 3a), and resonant electron flux (Figure 3e), and negatively correlates with the total magnetic field (Figure 3b) and the minimum resonant energy (Figure 3f).

[21] Figures 4a and 4b show the electron anisotropy $A(V_R)$ calculated using equation (3) and the ratio of resonant electrons to the total electrons $R(V_R)$ from equation (4) at three different wave frequencies respectively. The integrated wave amplitudes over the frequency ranges 0.05–0.15 f_{ce} (black), 0.15–0.25 f_{ce} (blue), and 0.25–0.35 f_{ce} (red) are shown in Figure 4c. For the whistler mode waves with frequencies of 0.1 and 0.2 f_{ce}, $A(V_R)$ remained almost constant during the wave enhancements suggesting that it is not the dominant factor that controls the chorus modulation. However, the observed whistler mode wave amplitude was remarkably well correlated with $R(V_R)$ at 0.1 and 0.2 f_{ce}, suggesting that it is $R(V_R)$ that plays the dominant role in controlling the local growth rate in Case 1. The wave amplitude at 0.3 f_{ce} was generally weak, since the measured anisotropy was similar but its growth requires higher $A(V_R)$ compared to waves with lower frequencies. For the wave with 0.3 f_{ce}, the observed wave amplitude became even weaker after 10:08 UT due to the small or occasionally even

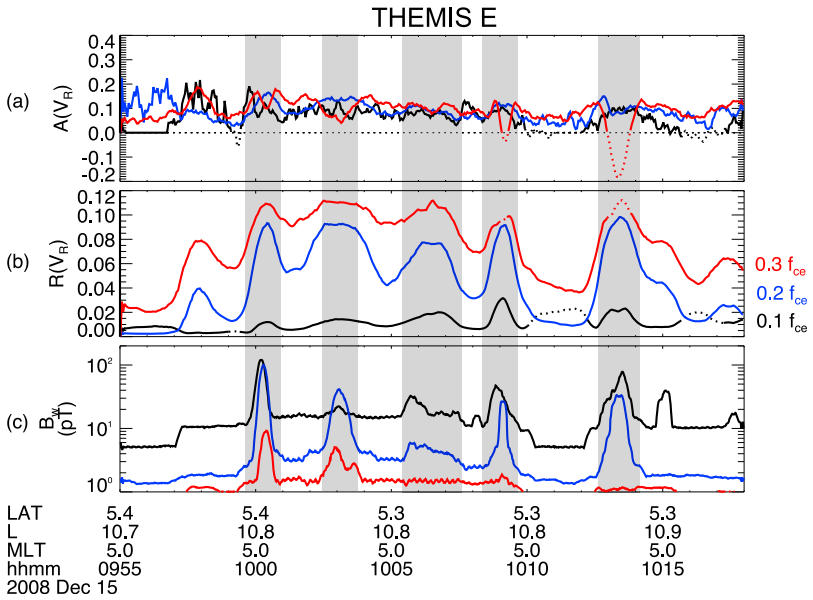

Figure 4. Case 1 observed by THEMIS E during the same period as in Figure 3. (a) Electron anisotropy $A(V_R)$ and (b) ratio of resonant electrons over total electrons $R(V_R)$ for three normalized wave frequencies. In Figures 4a and 4b, dotted line indicates the interval when $A(V_R) < 0$ for each corresponding frequency. (c) Integrated chorus wave amplitude over 0.05–0.15 f_{ce} (black), 0.15–0.25 f_{ce} (blue), and 0.25–0.35 f_{ce} (red).

negative $A(V_R)$, although $R(V_R)$ increased at ~10:09 and 10:13 UT. Here the calculated $A(V_R)$ may be underestimated probably due to the limited resolution of electron distribution data in pitch angle. Note that although the calculated anisotropy $A(V_R)$, compared to the critical anisotropy A_c (A_c is equal to 0.25 for the wave frequency of 0.2 f_{ce}), may appear to be insufficient to produce positive growth rates, it is nevertheless close to the value of the critical anisotropy. Even so, the trend of the electron anisotropy variation in the presence of Pc4–5 pulsations is realistic and indicates the approach to the onset of wave instability.

[22] In summary, in Case 1, which occurred at large L shells (>8) in the dawn sector, the substantial modulation of $R(V_R)$ caused by compressional Pc4–5 pulsations appears to play a dominant role in modulating whistler mode wave amplitudes, while the modulation of $A(V_R)$ is less significant.

4.2. Case 2

[23] Although compressional Pc4–5 pulsations are more commonly observed at large L shells of 8–12, they are occasionally observed at lower L shells [e.g., *Barfield and McPherron*, 1972; *Kremser et al.*, 1981; *Higbie et al.*, 1982; *Anderson et al.*, 1990; *Liu et al.*, 2009]. Figures 5a–5c show the solar wind dynamic pressure, IMF B_y and B_z, and AE index for such an event which occurred during 10:00–14:00 UT on 19 October 2008. The transparent red block in Figures 5a–5c represents the limited time period of Case 2, when particle burst data was available. Around this time, no substantial variation in solar wind dynamic pressure was observed. B_y remained negative with a slight change in magnitude, and B_z turned northward at ~12:50 UT just before the interval of Case 2. AE increased substantially at ~10:55 UT and became weaker after 12:40 UT. During this time interval of 10:00–14:00 UT, the geomagnetic activity was modest with Kp in the range 1 and 2 (not shown). Figures 5d–5g show parameters measured on THEMIS A in Case 2 between 12:54 and 13:02 UT, when particle burst data was available. Note that Case 2 occurred at lower L of ~6.6 in the dawn sector (~6.6 MLT). During this time interval, both the total electron density (Figure 5d) and the ambient magnetic field (Figure 5e) exhibited modest fluctuations with a time period of tens of seconds. In order to show the modulation of magnetic field more clearly, the band-pass filtered total magnetic field over 3–300 s is shown in Figure 5f. The modulation of the total electron density and magnetic field was out of phase, similar to Case 1. Figure 5g shows the magnetic pressure (blue), thermal pressure (black), and total pressure (red). In contrast to Case 1, the magnetic pressure was considerably larger than the thermal pressure, which indicates that these compressional pulsations are unlikely to be caused by drift mirror mode instability at the observed location, different from Case 1. A comparison to Figures 5a–5b shows that there was no apparent connection to external fluctuations originating in the solar wind during the time when the pulsation was observed. These compressional pulsations were probably observed after a period of substorm activity, consistent with the events shown by *Vaivads et al.* [2001]. We suggest that the occurrence of compressional pulsations near the geosynchronous orbit in Case 2 may reflect the results of substorm energization and injection of ion populations and therefore be driven internally by wave particle interactions, rather than directly by solar wind conditions.

[24] Figure 6 shows the key parameters responsible for the chorus wave modulation in Case 2 observed by THEMIS A. Figures 6a–6c show the same quantities as shown in Figures 5d–5f in order to compare with other key parameters for convenience. Figures 6d and 6e show electron energy fluxes and anisotropy (A^*) for the corresponding energy. The electron anisotropy was strongly dependent on

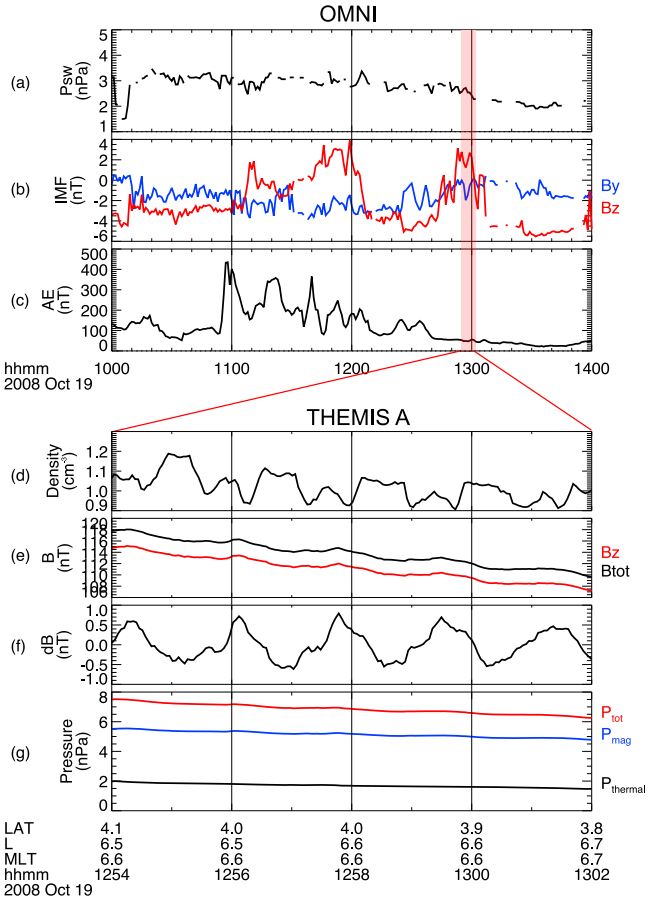

Figure 5. (a) Solar wind dynamic pressure, (b) IMF B_y and B_z and (c) AE during 10:00–14:00 UT on 19 October 2008. The transparent red block represents the time interval in Case 2 when particle burst data was available. (d) Total electron density, (e) total magnetic field (black) and magnetic field in the z direction in the SM coordinate (red), (f) band-pass filtered total magnetic field over 3–300 s, (g) thermal plasma pressure (black), magnetic pressure (blue), and total pressure (red) observed by THEMIS A during 12:54–13:02 UT, when particle burst data was available.

energy; it was larger (>0.8) in the energy range of 0.1–0.3 keV and 10–30 keV, but smaller (<~0.7) in the energy range of 0.3–10 keV and >30 keV. Figure 6f shows the electron energy flux over the energy range of 3–30 keV both perpendicular (blue) and parallel (black) to the ambient magnetic field. These electron fluxes include the main population of electrons resonating with chorus waves, since the minimum resonant energy is comparable to or larger than ~3 keV for observed chorus waves. The modulation of the electron energy flux (Figure 6f) was in antiphase with the background magnetic field and in phase with the total electron density. Figure 6g shows the minimum resonant energy of electrons interacting with chorus waves with frequencies of 0.4 and 0.55 f_{ce}. The modulation of the resonant energy in Case 2 was not as substantial as that in Case 1, predominantly due to much weaker relative variation of the ambient magnetic field (dB/B) at lower L shells, where the background magnetic field is larger. The frequency-time spectrogram of the wave magnetic field spectral intensity is shown in Figure 6i. Both lower band and upper band chorus waves were observed and the main power of chorus waves was observed at a frequency larger than ~0.35 f_{ce}. Wave burst data (which was available between 13:00:39 and 13:00:43 UT) with much higher resolution in frequency and time (not shown here) clearly shows the discrete emission of lower band and upper band chorus with a gap at 0.5 f_{ce}, and the main portion of wave power over the frequency range of 0.35–0.45 f_{ce}, even though the gap is not evident in the wave spectrum shown in Figure 6i due to limited resolution in frequency. The wave amplitudes of lower band and upper band chorus waves were obtained by integrating the wave magnetic field spectral intensity over the frequency band of 0.05–0.5 (blue) and 0.5–0.8 f_{ce} (red) and are shown in Figure 6h. The modulation of lower band chorus waves was generally in phase with the total electron density (Figure 6a) and in antiphase with the band-pass filtered magnetic field (Figure 6c). Interestingly, Figure 6h shows a phase difference between peaks of wave amplitude in lower band and upper band chorus.

[25] Figures 7a and 7b show the variation of $A(V_R)$ and $R(V_R)$ for the waves with frequencies of 0.4 (blue) and 0.55 f_{ce} (red) based on measured parameters by THEMIS A. Figure 7c shows wave amplitudes of lower band and upper band chorus, same as Figure 6h. Here upper band chorus was much weaker with B_w <10 pT compared to the lower band chorus, whose amplitude reached up to ~30 pT. In Figure 7a $A(V_R)$ exhibited substantial modulations at 0.4 f_{ce} from 0.1 to 0.3, whereas for the upper band chorus (~0.55 f_{ce}) $A(V_R)$ varied only between 0.4 and 0.5. Furthermore, the modulations of $A(V_R)$ for waves with frequencies of 0.4 and 0.55 f_{ce} were roughly out of phase, with larger values at 0.55 f_{ce}. $R(V_R)$ slightly varied during this period but the modulation was not as substantial as that in Case 1 primarily due to the larger background magnetic field compared to the small perturbation caused by compressional pulsations. The comparison of Figures 7a–7c indicates that the modulation of lower band chorus wave amplitude was generally in phase with $A(V_R)$, but exhibited little correlation with $R(V_R)$. Although the wave amplitude of the upper band chorus was weak, it was also modulated roughly in phase with the variation of $A(V_R)$. The approximate anticorrelation in $A(V_R)$ between lower band and upper band chorus shown in Figure 7a probably results in the approximate antiphase modulation in the wave amplitude between lower band and upper band chorus.

[26] In Case 2 compressional pulsations occurred at lower L shells, and thus the modulation of the magnetic field caused by compressional pulsations was much weaker compared to the background values. Consequently, the modulation of $R(V_R)$ (<~20%) was not substantial. However, the slight modulation of minimum resonant energy plays a significant role in modulating $A(V_R)$, since electron anisotropy (A^*) changed substantially near the resonant energy at ~10 keV, as shown in Figure 6e. In summary, in Case 2 which occurred at low L shells (~6.6) in the dawn sector, the modulation of $A(V_R)$ related to compressional Pc4–5 pulsations appears to play a dominant role in modulating whistler mode wave amplitude, when the modulation of $R(V_R)$ is less significant.

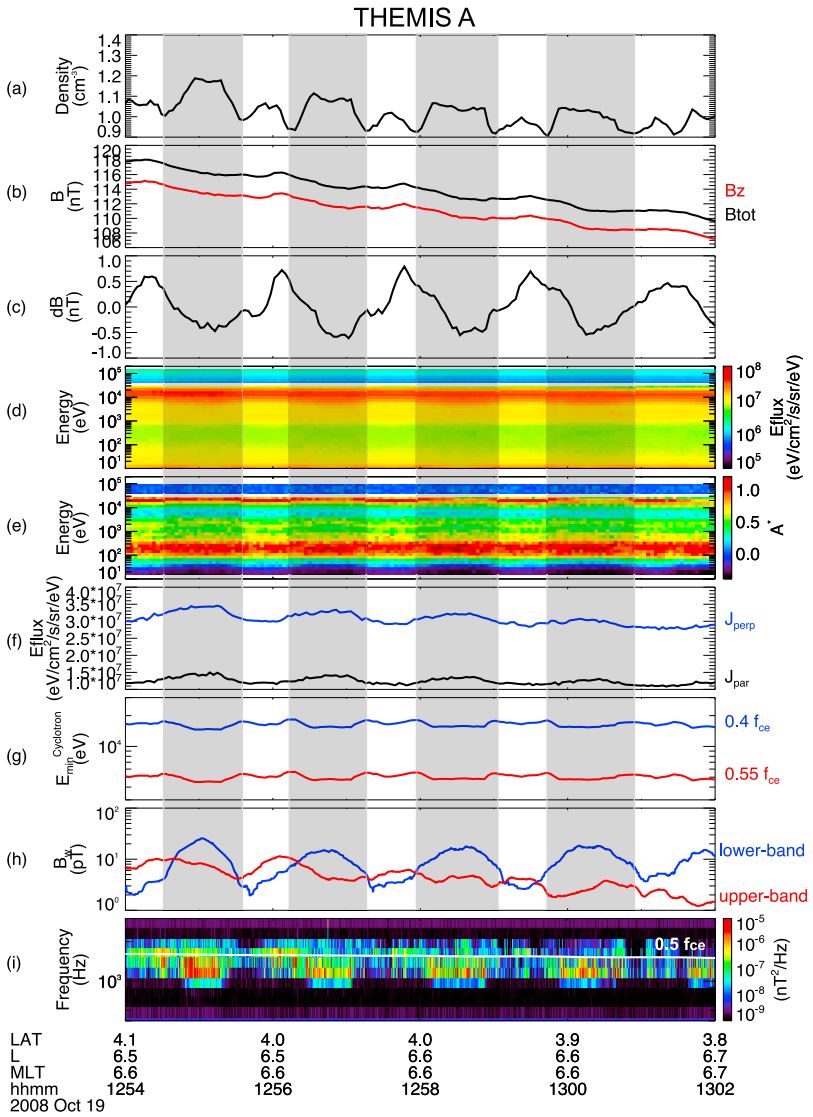

Figure 6. Case 2 observed by THEMIS A during the same period as in Figures 5d–5g. (a–c) Same as Figures 5d–5f. (d) Omnidirectional electron energy flux, and (e) electron anisotropy (A^*) as functions of energy and time. (f) Electron energy flux over the energy of 3–30 keV perpendicular (blue) and parallel (black) to the background magnetic field and (g) minimum resonant energy of electrons interacting with waves of 0.4 and 0.55 f_{ce} through the first-order cyclotron resonance. (h) Integrated lower band (blue) and upper band (red) chorus wave amplitude over 0.05–0.5 and 0.5–0.8 f_{ce} respectively. (i) Time-frequency spectrogram of the wave magnetic field spectral intensity and the white solid line represents 0.5 f_{ce}.

4.3. Statistical Result

[27] In order to comprehensively investigate the role of compressional Pc4–5 pulsations with an antiphase relationship between the total electron density and magnetic field in whistler mode wave modulation, we analyzed all events between 1 June 2008 and 1 August 2010, observed by the three inner probes of THEMIS A, D, and E. During this time interval, the THEMIS spacecraft spanned through all MLTs almost evenly, thus providing excellent coverage in MLT. Since compressional Pc4–5 pulsations predominantly occur at larger L shells and apogees of the three inner probes are ~12 R_E, we performed a statistical analysis in regions with a wide range of L shells between 5 and 12 and at all MLTs. Here we used the filter bank wave magnetic field data, which is available most of the time, to perform the statistical survey.

[28] Events have been selected by visual inspection using the physical quantities shown in Figure 2 and were required to satisfy the following criteria regardless of the generation mechanism of compressional Pc4–5 pulsations. First, the maximum wave amplitude of whistler mode waves (B_w shown in Figure 2g) during a 1 h time interval exceeds 10 pT in order to select waves with sufficiently large amplitudes. Second, the total electron density and the perturbation of the magnetic field are required to be out of phase with a period of tens of seconds to a few minutes. Third, the modulation of whistler mode wave amplitude positively correlates with the electron density and negatively corre-

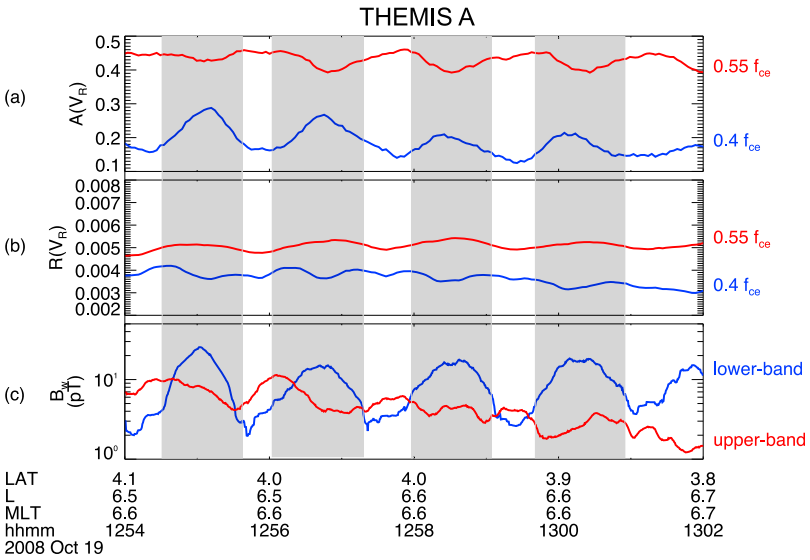

Figure 7. Case 2 observed by THEMIS A during the same period as in Figure 6. (a) $A(V_R)$ and (b) $R(V_R)$ for the normalized wave frequency of 0.4 (blue) and 0.55 f_{ce}. (c) Integrated lower band (blue) and upper band (red) chorus wave amplitude over 0.05–0.5 and 0.5–0.8 f_{ce} respectively.

lates with the background magnetic field. Finally, the spacecraft is located outside the plasmapause and inside the magnetopause. The location of the plasmapause is determined using the method described by *Li et al.* [2010b]. An event occurring during a 1 h interval and satisfying the above four criteria at least for ~10 min is counted as one event. We found 628 events in total during the period between 1 June 2008 and 1 August 2010. Although these 628 events have not been specifically sorted into the modulation by $R(V_R)$ or $A(V_R)$, most events (>620) were mainly caused by the modulation of $R(V_R)$ particularly at large L shells (>~8) and only a few events were clearly found to be dominantly modulated by $A(V_R)$ variations at lower L shells (<~8). We have also recorded the number of samples in order to provide the information on all available data samples. The L shell and MLT of each sample and event were recorded at the center of each 1 h time interval outside the plasmapause and inside the magnetopause during the same time period between 1 June 2008 and 1 August 2010. The number of samples and events were binned as a function of L in steps of 1 L and MLT with an interval of 1 h and are shown in Figure 8.

[29] Figure 8 shows the global distribution of the location of events (Figure 8a), number of samples (Figure 8b), number of events (Figure 8c), and occurrence rates of the event between 5 and 12 R_E at all MLT (Figure 8d). The occurrence rate was obtained by the ratio of the number of events to the number of samples in each bin. The majority of the events occurred at larger L shells (8–12) in the dawn sector, with a small fraction in the noon and dusk sectors. The number of samples was larger at higher radial distances. Because the absolute bin size (1 L × 1 MLT) is bigger due to the larger azimuthal size at higher L shells and the velocity of the spacecraft is smaller as the satellites become closer to apogee. Therefore, the time each spacecraft spent in each bin is longer and the number of samples is larger at higher L shells. We also note that the number of samples at larger L shells on the dayside was smaller compared to other MLT, since the magnetopause is closer to the Earth on the dayside (with <10 R_E during active times) and the data outside the magnetopause was excluded in this statistical survey.

[30] Figures 8c and 8d show that the events of modulation of whistler mode waves by compressional Pc4–5 pulsations mainly occurred at large L shells (>8) in the dawn sector between 3 and 8 MLT. Although compressional pulsations occur both in the dawn and dusk sectors [e.g., *Baumjohann et al.*, 1987; *Takahashi et al.*, 1990; *Zhu and Kivelson*, 1991], electron fluxes which provide the source of free energy for the generation of whistler mode waves are much lower in the dusk sector compared to those in the dawn sector [e.g., *Bortnik et al.*, 2007; *Li et al.*, 2010a]. Therefore, the occurrence rate of events in the dusk sector is much smaller than that in the dawn sector. Interestingly, the occurrence rate in the dawn sector was larger at higher L shells, probably due to the more significant variation of dB/B at higher L shells. Modulation of whistler mode waves by compressional Pc4–5 pulsations was much less commonly observed on the dayside and nightside possibly due to the much lower occurrence of compressional pulsations compared to that in the dawn and dusk flanks [e.g., *Hedgecock*, 1976; *Baumjohann et al.*, 1987; *Takahashi et al.*, 1990; *Anderson et al.*, 1990; *Zhu and Kivelson*, 1991; *Vaivads et al.*, 2000, 2001].

5. Discussion

[31] We focus on the role of compressional Pc4–5 pulsations exhibiting an anticorrelation between the total density and the background magnetic field in triggering the onset of chorus intensification. This type of compressional waves is associated with an increase in density, a decrease in background magnetic field, and a simultaneous increase in resonant electron flux, all of which provide favorable conditions for chorus wave generation. Other types of Pc4–5 compressional pulsations, such as fast mode waves with an in-phase correlation between the density and the back-

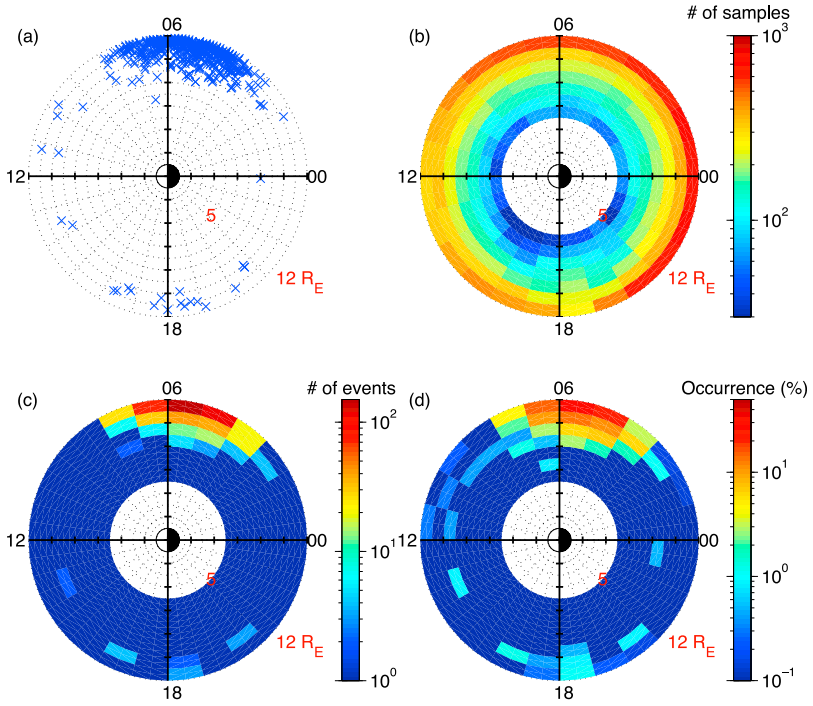

Figure 8. Global distributions of (a) the location of events, (b) number of samples, (c) number of events, and (d) the occurrence rate (%) of the events in regions of 5 and 12 R_E at all MLTs.

ground magnetic field, were probably not correlated well with the chorus amplitude. Those pulsations may be less efficient in modulating linear growth rates of chorus waves, since the in-phase variations of the two parameters diminish the net variations in minimum resonant energy.

[32] Using measured parameters from THEMIS, we evaluated the evolution of electron anisotropy $A(V_R)$ and the fractional density of resonant electrons $R(V_R)$, which contribute to the linear growth rates of whistler mode waves and compared the results to the observed wave amplitudes. $A(V_R)$ and/or $R(V_R)$ exhibited significant enhancements during intervals of chorus intensification, implying that linear theory can qualitatively describe the onset of wave instability. Energetic electron distributions are rapidly reduced to a state of marginal stability following injections from the plasma sheet during enhanced convection, as suggested by *Kennel and Petschek* [1966]. On the other hand, electron anisotropy in the energy range between a few hundred eV and ~100 keV exhibits positive values in the chorus dominant region [*Li et al.*, 2010a]. The onset of instability, as injected electrons drift to the dayside, is then triggered by macroscopic changes in the background plasma. Linear growth is important for small amplitude chorus and also plays a dominant role in the early stage of wave generation process for strong chorus waves [e.g., *Devine et al.*, 1995; *Omura et al.*, 2008]. Furthermore, linear growth rates provide essential information on whether the conditions in the plasma exceed the marginal stability allowing waves to grow to observable levels. However, nonlinear wave growth tends to play an important role after the linear growth phase particularly for the large amplitude waves, by rapidly increasing the wave amplitude followed by its saturation [e.g., *Omura and Summers*, 2004; *Omura et al.*, 2008]. Evaluation of nonlinear growth rates is beyond the scope of this study, but is important in simulating more realistic whistler mode wave spectrum.

[33] In the present study changes in the local growth rates of whistler mode waves were evaluated by computing $R(V_R)$ and $A(V_R)$ separately due to the reasons below. First, the values of $A(V_R)$ may be underestimated due to the limited resolution in pitch angle of measured electron distributions from ESA. Therefore, although the calculated anisotropies may appear to be insufficient to produce positive growth rates, they are nevertheless close to the values for marginal stability. Even so, the trend of the electron anisotropy variation in the presence of Pc4–5 pulsations is realistic and indicates the approach to the onset of wave instability. Second, the separate evaluation of $R(V_R)$ and $A(V_R)$ allows us to identify the dominant factor of the modulation of whistler mode waves in different source regions and under various generation conditions. $R(V_R)$ modulation tends to be dominant once changes in both total electron density and magnetic field with an antiphase are substantial under the condition that $A(V_R)$ is constantly sufficient. On the other hand, $A(V_R)$ modulation becomes dominant when variations in both total electron density and magnetic field are modest or small but the electron anisotropy changes substantially near the resonant energy.

[34] We used two kinds of definition for electron anisotropy shown in equations (3) and (6). The definition from equation (6) is for a fixed kinetic energy and is used to show the evolution of the electron pitch angle distribution for different energy levels. However, the linear wave growth rates are directly dependent on the electron anisotropy for the resonant parallel energy defined by equation (3), since the linear growth rates for a fixed frequency are evaluated

by an integration over the resonance ellipses [e.g., *Kennel and Petschek*, 1966; *Horne and Thorne*, 2003].

[35] In the absence of fresh electron injection events, the suprathermal population of electrons in the region exterior to the plasmapause appears to approach a state of marginal stability [e.g., *Kennel and Petschek*, 1966]. Under such conditions chorus instability can be modulated by variations in the background plasma properties caused by compressional Pc4–5 pulsations. In the present study we focused on the modulation of whistler mode waves by long period compressional pulsations in the Pc4–5 range. We did not investigate individual chorus elements, but rather a group of chorus elements showing intensification over a timescale of tens of seconds to a few minutes. However, whistler mode chorus can also be modulated over a much shorter time period (a few seconds to tens of seconds). In the companion paper *Li et al.* [2011], we discuss the potential mechanism of chorus modulation on this shorter timescale.

6. Summary and Conclusions

[36] We have investigated the role of compressional Pc4–5 pulsations with an antiphase relation between the total electron density and magnetic field in the modulation of whistler mode waves using THEMIS data in the near-equatorial magnetosphere. We have also evaluated the effect of variations in the fractional number of resonant electrons $R(V_R)$ and the resonant electron anisotropy $A(V_R)$ on linear growth rates of whistler mode waves using measured plasma parameters and compared the results to the observed wave amplitudes. The principal conclusions of our study can be summarized as follows.

[37] 1. Macroscopic compressional Pc4–5 pulsations associated with antiphase variations in density and magnetic field are particularly effective in triggering the onset of whistler mode instability by modulating resonant electron flux and electron anisotropy responsible for the chorus excitation on a timescale from tens of seconds to a few minutes. Whistler mode wave amplitude increases, as the ambient magnetic field decreases, the total electron density increases, and the resonant electron flux increases (and vice versa).

[38] 2. In the outer magnetosphere ($L > 8$), the modulation of $R(V_R)$ caused by compressional Pc4–5 pulsations is substantial and plays a dominant role in controlling variations in whistler wave linear growth rates, which leads to a pronounced modulation in chorus wave amplitudes.

[39] 3. In the inner magnetosphere ($L < 8$), the modulation of $R(V_R)$ caused by compressional Pc4–5 pulsations is less significant due to the smaller variation of the magnetic field compared to the background values. Consequently, the modulation of $A(V_R)$ could be the dominant mechanism of modulating the onset of chorus instability.

[40] 4. The modulation of whistler mode waves by compressional Pc4–5 pulsations preferentially occurs at large L shells (>8) in the dawn sector between 3 and 8 MLT and is dominantly caused by $R(V_R)$ variations. A much smaller fraction of events are associated with $A(V_R)$ modulations at lower L shells (<~8).

[41] **Acknowledgments.** This research was funded by the NSF grants AGS-0840178 and ATM-0802843, NASA Heliophysics Theory Program grant NNX08A135G, and NASA NAS5–02099. The authors acknowledge A. Roux and O. Le Contel for use of SCM data; J. W. Bonnell and F. S. Mozer for use of EFI data; C. W. Carlson and J. P. McFadden for use of ESA data; D. Larson and R. P. Lin for use of SST data; and K. H. Glassmeier, U. Auster, and W. Baumjohann for the use of FGM data provided under the lead of the Technical University of Braunschweig and with financial support through the German Ministry for Economy and Technology and the German Center for Aviation and Space (DLR) under contract 50 OC 0302. The authors also thank World Data Center for Geomagnetism, Kyoto for providing the *AE* index and OMNIWeb for the IMF and solar wind data.

[42] Robert Lysak thanks Nigel Meredith and the other reviewer for their assistance in evaluating this paper.

References

Anderson, B. J., M. J. Engebretson, S. P. Rounds, L. J. Zanetti, and T. A. Potemra (1990), A statistical study of Pc 3–5 pulsations observed by the AMPTE/CCE magnetic fields experiment: 1. Occurrence distributions, *J. Geophys. Res.*, *95*, 10,495–10,523.

Angelopoulos, V. (2008), The THEMIS mission, *Space Sci. Rev.*, *141*, 5–34, doi:10.1007/s11214-008-9336-1.

Auster, H. U., et al. (2008), The THEMIS fluxgate magnetometer, *Space Sci. Rev.*, *141*, 235–264, doi:10.1007/s11214-008-9365-9.

Barfield, J. N., and R. L. McPherron (1972), Statistical characteristics of storm-associated Pc 5 micropulsations observed at the synchronous equatorial orbit, *J. Geophys. Res.*, *77*, 4720–4733, doi:10.1029/JA077i025p04720.

Baumjohann, W., N. Sckopke, J. LaBelle, B. Klecker, H. Lühr, and K. H. Glassmeier (1987), Plasma and field observations of a compressional Pc 5 wave event, *J. Geophys. Res.*, *92*, 12,203–12,212.

Bespalov, P. A., M. Parrot, and J. Manninen (2010), Short-period VLF emissions as solitary envelope waves in a magnetospheric plasma maser, *J. Atmos. Sol. Terr. Phys.*, *72*(17), 1275–1281, doi:10.1016/j.jastp.2010.09.001.

Bonnell, J. W., F. S. Mozer, G. T. Delory, A. J. Hull, R. E. Ergun, C. M. Cully, V. Angelopoulos, and P. R. Harvey (2008), The Electric Field Instrument (EFI) for THEMIS, *Space Sci. Rev.*, *141*, 303–341, doi:10.1007/s11214-008-9469-2.

Bortnik, J., R. M. Thorne, and N. P. Meredith (2007), Modeling the propagation characteristics of chorus using CRRES suprathermal electron fluxes, *J. Geophys. Res.*, *112*, A08204, doi:10.1029/2006JA012237.

Burtis, W. J., and R. A. Helliwell (1969), Banded chorus—A new type of VLF radiation observed in the magnetosphere by OGO 1 and OGO 3, *J. Geophys. Res.*, *74*, 3002–3010, doi:10.1029/JA074i011p03002.

Chen, M. W., J. L. Roeder, J. F. Fennell, L. R. Lyons, R. L. Lambour, and M. Schulz (1999), Proton ring current pitch angle distributions: Comparison of simulations with CRRES observations, *J. Geophys. Res.*, *104*, 17,379–17,389, doi:10.1029/1999JA900142.

Cheng, C. Z., and C. S. Lin (1987), Eigenmode analysis of compressional waves in the magnetosphere, *Geophys. Res. Lett.*, *14*, 884–887, doi:10.1029/GL014i008p00884.

Coroniti, F. V., and C. F. Kennel (1970), Electron precipitation pulsations, *J. Geophys. Res.*, *75*, 1279–1289, doi:10.1029/JA075i007p01279.

Cully, C. M., R. E. Ergun, K. Stevens, A. Nammari, and J. Westfall (2008), The THEMIS digital fields board, *Space Sci. Rev.*, *141*, 343–355, doi:10.1007/s11214-008-9417-1.

Devine, P. E., S. C. Chapman, and J. W. Eastwood (1995), One- and two-dimensional simulations of whistler mode waves in an anisotropic plasma, *J. Geophys. Res.*, *100*, 17,189–17,203, doi:10.1029/95JA00842.

Han, D.-S., H.-G. Yang, Z.-T. Chen, T. Araki, M. W. Dunlop, M. Nosé, T. Iyemori, Q. Li, Y.-F. Gao, and K. Yumoto (2007), Coupling of perturbations in the solar wind density to global Pi3 pulsations: A case study, *J. Geophys. Res.*, *112*, A05217, doi:10.1029/2006JA011675.

Hasegawa, A. (1969), A drift mirror instability in the magnetosphere, *Phys. Fluids*, *12*, 2642–2650, doi:10.1063/1.1692407.

Hedgecock, P. C. (1976), Giant Pc4–5 pulsations in the outer magnetosphere: A survey of Heos-1 data, *Planet. Space Sci.*, *24*, 921–935, doi:10.1016/0032-0633(76)90003-9.

Helliwell, R. A. (1965), *Whistlers and Related Ionospheric Phenomena*, Stanford Univ. Press, Stanford, Calif.

Helliwell, R. A. (1967), A theory of discrete emissions from the magnetosphere, *J. Geophys. Res.*, *72*, 4773–4790, doi:10.1029/JZ072i019p04773.

Higbie, P. R., D. N. Baker, R. D. Zwickl, R. D. Belian, J. R. Asbridge, J. F. Fennell, B. Wilken, and C. W. Arthur (1982), The global Pc 5 event of November 14–15, 1979, *J. Geophys. Res.*, *87*, 2337–2345, doi:10.1029/JA087iA04p02337.

Horne, R. B., and R. M. Thorne (2003), Relativistic electron acceleration and precipitation during resonant interactions with whistler-mode chorus, *Geophys. Res. Lett.*, *30*(10), 1527, doi:10.1029/2003GL016973.

Hughes, W. J., and D. J. Southwood (1976), The screening of micropulsation signals by the atmosphere and ionosphere, *J. Geophys. Res.*, *81*, 3234–3240, doi:10.1029/JA081i019p03234.

Kennel, C. F., and H. E. Petschek (1966), Limit on stable trapped particle fluxes, *J. Geophys. Res.*, *71*, 1–28.
Kennel, C. F., and R. M. Thorne (1967), Unstable growth of unducted whistlers propagating at an angle to the geomagnetic field, *J. Geophys. Res.*, *72*, 871–878, doi:10.1029/JZ072i003p00871.
Kepko, L., and H. E. Spence (2003), Observations of discrete, global magnetospheric oscillations directly driven by solar wind density variations, *J. Geophys. Res.*, *108*(A6), 1257, doi:10.1029/2002JA009676.
Kessel, R. L. (2008), Solar wind excitation of Pc4–5 fluctuations in the magnetosphere and on the ground, *J. Geophys. Res.*, *113*, A04202, doi:10.1029/2007JA012255.
Kimura, I. (1974), Interrelation between VLF and ULF emissions, *Space Sci. Rev.*, *16*, 389–411, doi:10.1007/BF00171565.
Kivelson, M. G., and D. J. Southwood (1996), Mirror instability II: The mechanism of nonlinear saturation, *J. Geophys. Res.*, *101*, 17,365–17,371, doi:10.1029/96JA01407.
Kokubun, S., M. G. Kivelson, R. L. McPherron, C. T. Russell, and H. I. West Jr. (1977), Ogo 5 observations of Pc 5 waves: Particle flux modulations, *J. Geophys. Res.*, *82*, 2774–2786, doi:10.1029/JA082i019p02774.
Koons, H. C., and J. L. Roeder (1990), A survey of equatorial magnetospheric wave activity between 5 and 8 R(E), *Planet. Space Sci.*, *38*, 1335–1341, doi:10.1016/0032-0633(90)90136-E.
Korotova, G. I., D. G. Sibeck, B. Kondratovich, V. Angelopoulos, and O. D. Constantinescu (2009), THEMIS observations of compressional pulsations in the dawn-side magnetosphere: A case study, *Ann. Geophys.*, *27*, 3725–3735, doi:10.5194/angeo-27-3725-2009.
Kremser, G., A. Korth, J. A. Fejer, B. Wilken, A. V. Gurevich, and E. Amata (1981), Observations of quasi-periodic flux variations of energetic ions and electrons associated with Pc 5 geomagnetic pulsations, *J. Geophys. Res.*, *86*, 3345–3356, doi:10.1029/JA086iA05p03345.
Lampe, M., J. Glenn, W. M. Manheimer, and G. Guanuli (2010), Nonlinear whistler instability driven by a beamlike distribution of resonant electrons, *Phys. Plasmas*, *17*, 022902, doi:10.1063/1.3298733.
Lauben, D. S., U. S. Inan, T. F. Bell, and D. A. Gurnett (2002), Source characteristics of ELF/VLF chorus, *J. Geophys. Res.*, *107*(A12), 1429, doi:10.1029/2000JA003019.
Le Contel, O., et al. (2008), First results of the THEMIS searchcoil magentometers, *Space Sci. Rev.*, *141*, 509–534, doi:10.1007/s11214-008-9371-y.
LeDocq, M. J., D. A. Gurnett, and G. B. Hospodarsky (1998), Chorus source locations from VLF Poynting flux measurements with the Polar spacecraft, *Geophys. Res. Lett.*, *25*(21), 4063–4066, doi:10.1029/1998GL900071.
Li, W., R. M. Thorne, N. P. Meredith, R. B. Horne, J. Bortnik, Y. Y. Shprits, and B. Ni (2008), Evaluation of whistler mode chorus amplification during an injection event observed on CRRES, *J. Geophys. Res.*, *113*, A09210, doi:10.1029/2008JA013129.
Li, W., R. M. Thorne, V. Angelopoulos, J. W. Bonnell, J. P. McFadden, C. W. Carlson, O. LeContel, A. Roux, K. H. Glassmeier, and H. U. Auster (2009a), Evaluation of whistler-mode chorus intensification on the nightside during an injection event observed on the THEMIS spacecraft, *J. Geophys. Res.*, *114*, A00C14, doi:10.1029/2008JA013554.
Li, W., R. M. Thorne, V. Angelopoulos, J. Bortnik, C. M. Cully, B. Ni, O. LeContel, A. Roux, U. Auster, and W. Magnes (2009b), Global distribution of whistler-mode chorus waves observed on the THEMIS spacecraft, *Geophys. Res. Lett.*, *36*, L09104, doi:10.1029/2009GL037595.
Li, W., et al. (2010a), THEMIS analysis of observed equatorial electron distributions responsible for the chorus excitation, *J. Geophys. Res.*, *115*, A00F11, doi:10.1029/2009JA014845.
Li, W., R. Thorne, J. Bortnik, Y. Nishimura, V. Angelopoulos, L. Chen, J. P. McFadden, and J. W. Bonnell (2010b), Global distributions of suprathermal electrons observed on THEMIS and potential mechanisms for access into the plasmasphere, *J. Geophys. Res.*, *115*, A00J10, doi:10.1029/2010JA015687.
Li, W., J. Bortnik, R. M. Thorne, Y. Nishimura, V. Angelopoulos, and L. Chen (2011), Modulation of whistler-mode chorus waves: 2. Role of density variations, *J. Geophys. Res.*, *116*, A06206, doi:10.1029/2010JA016313.
Liu, W., T. E. Sarris, X. Li, S. R. Elkington, R. Ergun, V. Angelopoulos, J. Bonnell, and K. H. Glassmeier (2009), Electric and magnetic field observations of Pc4 and Pc5 pulsations in the inner magnetosphere: A statistical study, *J. Geophys. Res.*, *114*, A12206, doi:10.1029/2009JA014243.
Manninen, J., N. G. Kleimenova, O. V. Kozyreva, and T. Turunen (2010), Pc5 geomagnetic pulsations, pulsating particle precipitation, and VLF chorus: Case study on 24 November 2006, *J. Geophys. Res.*, *115*, A00F14, doi:10.1029/2009JA014837.
McFadden, J. P., C. W. Carlson, D. Larson, V. Angelopoulos, M. Ludlam, R. Abiad, B. Elliott, P. Turin, and M. Marckwordt (2008), The THEMIS ESA plasma instrument and in-flight calibration, *Space Sci. Rev.*, *141*, 277–302, doi:10.1007/s11214-008-9440-2.
Meredith, N. P., R. B. Horne, R. M. Thorne, and R. R. Anderson (2003), Favored regions for chorus-driven electron acceleration to relativistic energies in the Earth's outer radiation belt, *Geophys. Res. Lett.*, *30*(16), 1871, doi:10.1029/2003GL017698.
Mozer, F. S. (1973), Analysis of techniques for measuring DC and AC electric fields in the magnetosphere, *Space Sci. Rev.*, *14*, 272–313, doi:10.1007/BF02432099.
Nunn, D., Y. Omura, H. Matsumoto, I. Nagano, and S. Yagitani (1997), The numerical simulation of VLF chorus and discrete emissions observed on the Geotail satellite using a Vlasov code, *J. Geophys. Res.*, *102*, 27,083–27,097, doi:10.1029/97JA02518.
Omura, Y., and D. Summers (2004), Computer simulations of relativistic whistler-mode wave-particle interactions, *Phys. Plasmas*, *11*, 3530, doi:10.1063/1.1757457.
Omura, Y., Y. Katoh, and D. Summers (2008), Theory and simulation of the generation of whistler-mode chorus, *J. Geophys. Res.*, *113*, A04223, doi:10.1029/2007JA012622.
Omura, Y., M. Hikishima, Y. Katoh, D. Summers, and S. Yagitani (2009), Nonlinear mechanisms of lower-band and upper-band VLF chorus emissions in the magnetosphere, *J. Geophys. Res.*, *114*, A07217, doi:10.1029/2009JA014206.
Patel, V. L., P. H. Ng, and L. J. Cahill Jr. (1983), Drift wave model for geomagnetic pulsations in a high β plasma, *J. Geophys. Res.*, *88*, 5677–5684, doi:10.1029/JA088iA07p05677.
Pedersen, A., F. Mozer, and G. Gustafsson (1998), Electric field measurements in a tenuous plasma with spherical double probes, in *Measurement Techniques in Space Plasmas: Fields*, *Geophys. Monogr. Ser.*, vol. 103, edited by J. Borovsky, R. Pfaff, and A. Young, pp. 1–12, AGU, Washington, D. C.
Price, C. P., D. W. Swift, and L.-C. Lee (1986), Numerical simulation of nonoscillatory mirror waves at the Earth's magnetosheath, *J. Geophys. Res.*, *91*, 101–112, doi:10.1029/JA091iA01p00101.
Rae, I. J., I. R. Mann, C. E. J. Watt, L. M. Kistler, and W. Baumjohann (2007), Equator-S observations of drift mirror mode waves in the dawn-side magnetosphere, *J. Geophys. Res.*, *112*, A11203, doi:10.1029/2006JA012064.
Roux, A., O. Le Contel, C. Coillot, A. Bouabdellah, B. de la Porte, D. Alison, S. Ruocco, and M. C. Vassal (2008), The search coil magnetometer for THEMIS, *Space Sci. Rev.*, *141*, 265–275, doi:10.1007/s11214-008-9455-8.
Santolík, O., D. A. Gurnett, J. S. Pickett, M. Parrot, and N. Cornilleau-Wehrlin (2003), Spatio-temporal structure of storm-time chorus, *J. Geophys. Res.*, *108*(A7), 1278, doi:10.1029/2002JA009791.
Santolík, O., D. Gurnett, and J. Pickett (2004), Multipoint investigation of the source region of storm-time chorus, *Ann. Geophys.*, *22*, 2555–2563, doi:10.5194/angeo-22-2555-2004.
Santolík, O., et al. (2010), Wave-particle interactions in the equatorial source region of whistler-mode emissions, *J. Geophys. Res.*, *115*, A00F16, doi:10.1029/2009JA015218.
Sarris, T. E., T. M. Loto'aniu, X. Li, and H. J. Singer (2007), Observations at geosynchronous orbit of a persistent Pc4–5 geomagnetic pulsation and energetic electron flux modulations, *Ann. Geophys.*, *25*, 1653–1667, doi:10.5194/angeo-25-1653-2007.
Sato, N., and H. Fukunishi (1981), Interaction between ELF-VLF emissions and magnetic pulsations: Classification of quasi-periodic ELF-VLF emissions based on frequency-time spectra, *J. Geophys. Res.*, *86*, 19–29, doi:10.1029/JA086iA01p00019.
Sato, N., K. Hayashi, S. Kokubun, T. Oguti, and H. Fukunishi (1974), Relationships between quasi-periodic VLF emission and geomagnetic pulsations, *J. Atmos. Terr. Phys.*, *36*, 1515–1516, doi:10.1016/0021-9169(74)90229-3.
Schriver, D., et al. (2010), Generation of whistler mode emissions in the inner magnetosphere: An event study, *J. Geophys. Res.*, *115*, A00F17, doi:10.1029/2009JA014932.
Sibeck, D. G., and V. Angelopoulos (2008), THEMIS science objectives and mission phases, *Space Sci. Rev.*, *141*, 35–59, doi:10.1007/s11214-008-9393-5.
Southwood, D. J., and M. G. Kivelson (1993), Mirror instability: 1. Physical mechanism of linear instability, *J. Geophys. Res.*, *98*, 9181–9187, doi:10.1029/92JA02837.
Spanswick, E., E. Donovan, and G. Baker (2005), Pc4–5 modulation of high energy electron precipitation: Particle interaction regions and scattering efficiency, *Ann. Geophys.*, *23*, 1533–1542, doi:10.5194/angeo-23-1533-2005.
Starks, M. J., R. A. Quinn, G. P. Ginet, J. M. Albert, G. S. Sales, B. W. Reinisch, and P. Song (2008), Illumination of the plasmasphere by terrestrial very low frequency transmitters: Model validation, *J. Geophys. Res.*, *113*, A09320, doi:10.1029/2008JA013112.
Takahashi, K., C. Z. Cheng, R. W. McEntire, and L. M. Kistler (1990), Observation and theory of Pc 5 waves with harmonically related transverse and compressional components, *J. Geophys. Res.*, *95*, 977–989, doi:10.1029/JA095iA02p00977.

Tixier, M., and N. Cornilleau-Wehrlin (1986), How are the VLF quasi-periodic emissions controlled by harmonics of field line oscillations? The results of a comparison between ground and Geos satellites measurements, *J. Geophys. Res.*, *91*, 6899–6919, doi:10.1029/JA091iA06p06899.

Tsurutani, B. T., and E. J. Smith (1974), Postmidnight chorus: A substorm phenomenon, *J. Geophys. Res.*, *79*, 118–127, doi:10.1029/JA079i001p00118.

Tsurutani, B. T., and E. J. Smith (1977), Two types of magnetospheric ELF chorus and their substorm dependences, *J. Geophys. Res.*, *82*, 5112–5128, doi:10.1029/JA082i032p05112.

Tsurutani, B. T., O. P. Verkhoglyadova, G. S. Lakhina, and S. Yagitani (2009), Properties of dayside outer zone chorus during HILDCAA events: Loss of energetic electrons, *J. Geophys. Res.*, *114*, A03207, doi:10.1029/2008JA013353.

Vaivads, A., G. Haerendel, W. Baumjohann, R. Nakamura, H. Kucharek, E. Georgescu, B. Klecker, and L. Kistler (2000), Compressional Pc4–5 pulsations as sloshing in the plasma sheet, *J. Geophys. Res.*, *105*, 23,287–23,292, doi:10.1029/2000JA900085.

Vaivads, A., W. Baumjohann, G. Haerendel, R. Nakamura, H. Kucharek, B. Klecker, M. R. Lessard, L. M. Kistler, T. Mukai, and A. Nishida (2001), Compressional Pc4–5 type pulsations in the morningside plasma sheet, *Ann. Geophys.*, *19*, 311–320, doi:10.5194/angeo-19-311-2001.

Vaivads, A., O. Santolík, G. Stenberg, M. André, C. J. Owen, P. Canu, and M. Dunlop (2007), Source of whistler emissions at the dayside magnetopause, *Geophys. Res. Lett.*, *34*, L09106, doi:10.1029/2006GL029195.

Zhu, X., and M. G. Kivelson (1991), Compressional ULF waves in the outer magnetosphere: 1. Statistical study, *J. Geophys. Res.*, *96*, 19,451–19,467.

Zhu, X., and M. G. Kivelson (1994), Compressional ULF waves in the outer magnetosphere: 2. A case study of Pc 5 type wave activity, *J. Geophys. Res.*, *99*, 241–252, doi:10.1029/93JA02106.

V. Angelopoulos, Institute of Geophysics and Planetary Physics, Department of Earth and Space Sciences, University of California, Los Angeles, CA 90095-1567, USA. (vassilis@ucla.edu)

J. Bortnik, W. Li, Y. Nishimura, and R. M. Thorne, Department of Atmospheric and Oceanic Sciences, University of California, 405 Hilgard Ave., Los Angeles, CA 90095-1565, USA. (jbortnik@gmail.com; moonli@atmos.ucla.edu; toshi@atmos.ucla.edu; rmt@atmos.ucla.edu)